CellPress

Chemistry & Biology
Article

Enzyme Inhibition by Hydroamination: Design and Mechanism of a Hybrid Carmaphycin-Syringolin Enone Proteasome Inhibitor

Daniela B.B. Trivella,[1,2,3,8] Alban R. Pereira,[1,8] Martin L. Stein,[4,8] Yusuke Kasai,[1] Tara Byrum,[1] Frederick A. Valeriote,[5] Dean J. Tantillo,[6] Michael Groll,[4,*] William H. Gerwick,[1,7,*] and Bradley S. Moore[1,7,*]

[1]Center for Marine Biotechnology and Biomedicine, Scripps Institution of Oceanography, University of California at San Diego, La Jolla, CA 92093-0212, USA

[2]Institute of Chemistry, University of Campinas, Campinas SP 13083-970, Brazil

[3]Brazilian Biosciences National Laboratory, National Center for Research in Energy and Materials, Campinas SP 13083-970, Brazil

[4]Center for Integrated Protein Science, Department Chemie, Lehrstuhl für Biochemie, Technische Universität München, Garching 85747, Germany

[5]Henry Ford Health System, Department of Internal Medicine, Josephine Ford Cancer Center, 440 Burroughs, Detroit, MI 48202, USA

[6]Department of Chemistry, University of California at Davis, 1 Shields Avenue, Davis, CA 95616, USA

[7]Skaggs School of Pharmacy and Pharmaceutical Sciences, University of California at San Diego, La Jolla, CA 92093-0736, USA

[8]Co-first author

*Correspondence: michael.groll@tum.de (M.G.), wgerwick@ucsd.edu (W.H.G.), bsmoore@ucsd.edu (B.S.M.)

http://dx.doi.org/10.1016/j.chembiol.2014.04.010

SUMMARY

Hydroamination reactions involving the addition of an amine to an inactivated alkene are entropically prohibited and require strong chemical catalysts. While this synthetic process is efficient at generating substituted amines, there is no equivalent in small molecule-mediated enzyme inhibition. We report an unusual mechanism of proteasome inhibition that involves a hydroamination reaction of alkene derivatives of the epoxyketone natural product carmaphycin. We show that the carmaphycin enone first forms a hemiketal intermediate with the catalytic Thr1 residue of the proteasome before cyclization by an unanticipated intramolecular alkene hydroamination reaction, resulting in a stable six-membered morpholine ring. The carmaphycin enone electrophile, which does not undergo a 1,4-Michael addition as previously observed with vinyl sulfone and α,β-unsaturated amide-based inhibitors, is partially reversible and gives insight into the design of proteasome inhibitors for cancer chemotherapy.

INTRODUCTION

Hydroamination of unactivated alkenes is a challenging process because such reactions are generally not very exothermic and are entropically disfavored (Beller et al., 2004; Hultzsch, 2005). In general, these reactions require protonation of the alkene π-bond, leading to a carbocation intermediate that is then attacked by the amine nucleophile (Beller et al., 2004). Whereas this process can be promoted by alkali, transition, or rare earth metals, as well as by Lewis or Brønsted acids and bases (Beller et al., 2004; Schlummer and Hartwig, 2002; Hultzsch, 2005), no equivalent in small molecule-mediated enzyme inhibition has been reported. The entropic penalty for a biochemical hydroamination reaction, however, may conceivably be overcome by preorganization in an enzyme reactive site. In this work, we report enzyme inhibition mediated by hydroamination using proteasome inhibitors derived from natural products. The scaffolds of these small molecules interact tightly with the protein, which facilitates hydroamination by the enzyme N-terminal amine.

The proteasome functions as the central hub of nonlysosomal cellular proteolysis where it mediates a number of key processes such as cell cycle control, cell differentiation, immune response, amino acid recycling, and apoptosis (Goldberg, 2007; Murata et al., 2009). These biological processes can thus be manipulated through the addition of small molecules that selectively target the proteolytically active β subunits of the proteasome (Kisselev et al., 2012; Moore et al., 2008; Borissenko and Groll, 2007). Due to the importance of the proteasome to malignant cells and the immune process, it is considered a biological target of high interest for pharmaceutical development. Two proteasome inhibitors, the epoxyketone carfilzomib (Kyprolis) and the peptide boronate bortezomib (Velcade), are now used clinically as anticancer agents and others are in development.

Several proteasome inhibitors have been reported from natural and synthetic sources and include both noncovalent and covalent inhibitors (Kisselev et al., 2012). The covalent proteasome inhibitors can display reversible or irreversible inhibition profiles and present, in most cases, a peptidic core and an electrophilic warhead. The peptidic core is responsible for forming a stable antiparallel β sheet with the enzyme, which in turn positions the warhead in ideal geometry for covalent attachment of the Thr1 proteasome catalytic residue. The Thr1 side chain oxygen (Thr1Oγ) is the nucleophile responsible for the attack on electrophilic substrates, including the natural peptidic substrate and several classes of inhibitor electrophiles, thus forming covalent adducts (Kisselev et al., 2012). Taking advantage of the inhibitor stability and warhead positioning conferred by the peptidic core of proteasome inhibitors, we used the recently discovered natural product carmaphycin (**1**; Pereira et al.,

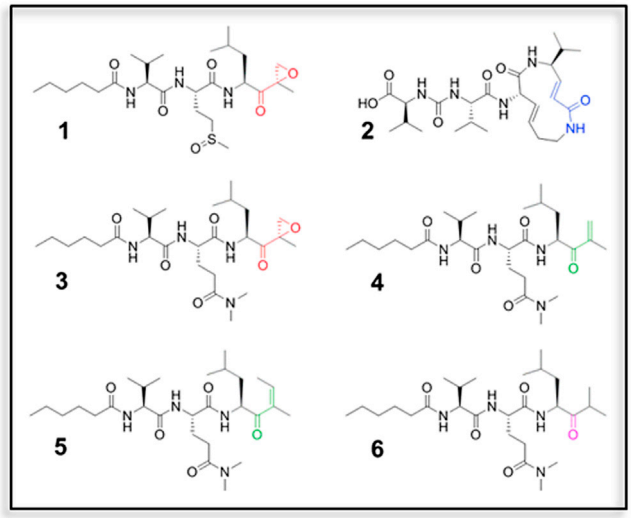

Figure 1. Natural Product Proteasome Inhibitors
Carmaphycin A (**1**), syringolin A (**2**), and derivatives **3–6**.

2012) and its derivatives (Figure 1) to challenge the Thr1 nucleophile in interacting with enone electrophiles.

Structurally, **1** features a leucine-derived α′,β′-epoxyketone warhead (the P1 residue) directly connected to a methionine sulfoxide (the P2 residue), which in turn is connected to a valine (the P3 residue) and an alkyl chain terminal tail (Figure 1). α′,β′-epoxyketones, as exemplified in **1**, the bacterial natural product epoxomicin (Groll et al., 2000; Meng et al., 1999), and its recently US Food and Drug Administration (FDA)-approved derivative carfilzomib (Molineaux, 2012) are potent, selective, and irreversible proteasome inhibitors. Epoxyketone warheads form stable morpholine derivatives with the active site Thr1 residues in the six proteolytic sites of the 20S proteasome core particle (Groll et al., 2000; Meng et al., 1999). The warhead carbonyl and epoxide undergo two successive nucleophilic attacks performed by Thr1Oγ and Thr1N, respectively (Groll et al., 2000).

Another class of proteasome inhibitor warheads of interest are α,β-unsaturated systems, such as α,β-unsaturated amides, as seen in the proteasome inhibitor and plant pathogen virulence factor syringolin A (Groll et al., 2008; **2**), and vinylsulfones (Kisselev et al., 2012). These undergo 1,4-Michael addition with the Thr1Oγ nucleophile, forming a one-step irreversible covalent adduct with Thr1Oγ.

We thus hypothesized that replacing the epoxyketone warhead in **1** with a complementary α,β-unsaturated carbonyl as in **2** would probe the plasticity of the proteasome and change the nature of the chemical reactions between the inhibitor and the enzyme. Herein we report an unusual mechanism of proteasome inhibition that involves a hydroamination reaction of alkene derivatives of the carmaphycin class of proteasome inhibitors.

RESULTS

Synthesis of Carmaphycin Derivatives

Due to the unstable redox properties of the methionine sulfoxide at the P2 residue position of natural carmaphycin A (**1**), we replaced this residue with *N,N*-dimethylglutamine. Based on alterations to our original total synthesis (Pereira et al., 2012) of **1**, we prepared epoxyketone **3**, enones **4** and **5**, and ketone **6**. These synthetic analogs along with natural product **1** were used in this study to explore and compare the relative inhibitory effect of different ketone derivatives in the carmaphycin series. The complete synthetic procedures are reported in the Supplemental Experimental Procedures and Experimental Procedures.

Table 1. Inhibitory Activity of Carmaphycin and Analogs as Measured in Human Cell Assays and with the Purified Yeast 20S Proteasome

	ChTL (β5)[a]	TL (β2)[b]	H-460[c]	HCT-116[d]
1	1.5 ± 0.2	46.2 ± 6.0	16.4 ± 2.7	19.4 ± 0.1
3	1.2 ± 0.1	112.4 ± 7.0	19.6 ± 2.4	10.7 ± 2.3
4	164.5 ± 5.6	>50,000	1,667.0 ± 82.0	727.4 ± 167.1

IC_{50} values (nM) are presented.
[a]Purified yeast proteasome, Suc-LLVY-Amc is a peptide substrate to specifically determine ChTL activity.
[b]Purified yeast proteasome, Ac-LRR-Amc is a peptide substrate to specifically determine TL activity.
[c]H-460 human lung cancer cell line.
[d]HCT-116 human colon cancer cell line.

Activity Assays

We first interrogated the chymotrypsin-like (ChTL) inhibitory activity of the carmaphycin analog **3** and measured a similar potency in comparison with the natural compound **1** (1.2 nM versus 1.5 nM with the purified proteasome, respectively), suggesting the functional similarity of their P2 residues (Table 1). We next analyzed the carmaphycin/syringolin chimera **4**, which also displayed high potency with nanomolar inhibition of the purified proteasome, albeit with a 100-fold loss in activity (164 nM). The proteasome trypsin-like activity (TL, β2 subunit) was also measured, showing preferable inhibitor binding to ChTL over TL for the three inhibitors tested. Overall, the relative potencies of ChTL inhibition matched the cell toxicity properties of these new derivatives, with compound **3** being of highest potency, whereas **4** displayed decreased activity yet still had effects in the nanomolar range (Table 1).

We further showed the importance of the alkene or epoxide groups in the warhead of these inhibitors by preparing and testing saturated ketone **6**. Compound **6** was not active in the enzyme nor in the cell-based assays, even at concentration as high as 1 mM.

To more fully explore the consequence of replacing the epoxyketone in **3** with the enone warhead in **4**, we separately incubated **1**, **3** and **4** with the yeast and human 20S proteasomes to measure their relative binding properties (Figures S1 and S2 available online). Compounds **1** and **3** showed a clear reversible mode of binding after 2 hr of incubation with the ligand (Figures S1A and S1D). However, the reversibility was less evident after 6 hr (Figures S1B and S1E) and after 24 hr was irreversible (Figures S1C and S1F). This inhibition profile suggests a two-step mechanism of interaction with the proteasome, much like that observed for the prototype epoxomicin (Groll et al., 2000; Meng et al., 1999), and is highly anticipated for epoxyketone warheads. Epoxyketones undergo a fast reversible inhibition

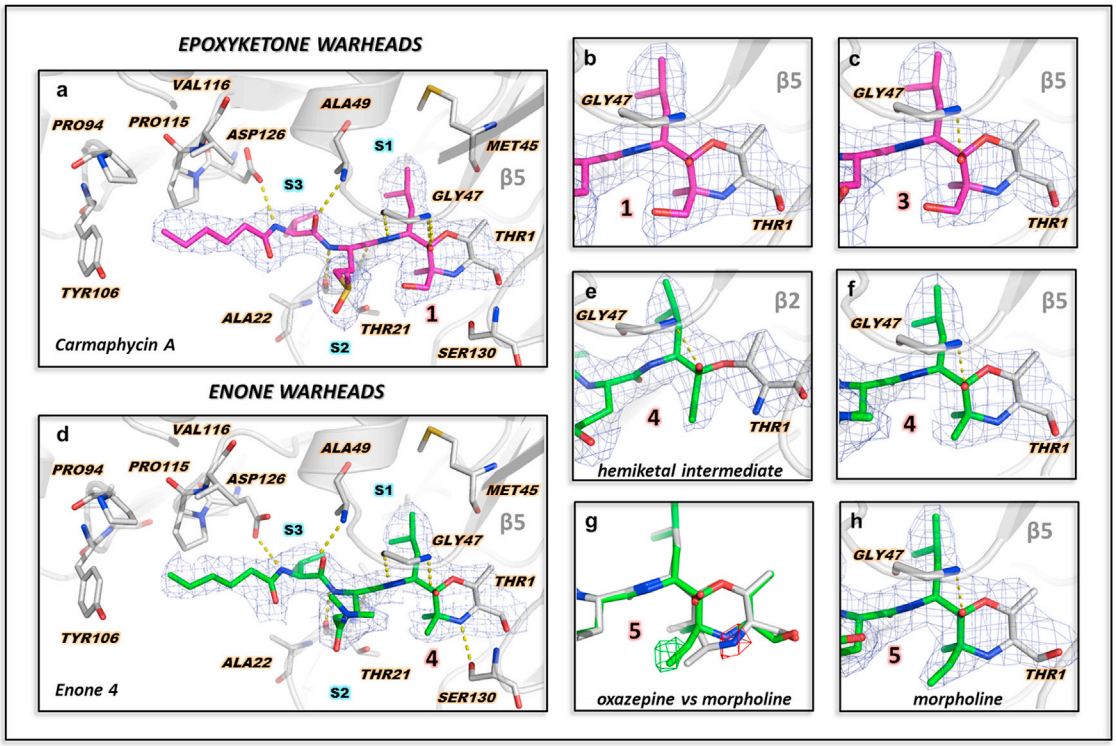

Figure 2. Crystal Structures of the Yeast 20S Proteasome Binding the Natural Product Carmaphycin A (1) and Derivatives Containing Epoxyketone and Enone Warheads

(A–H) General view of the ChTL catalytic unit binding **1** (A) and detailed view of **1** (B) and **3** (C) epoxyketone warheads. The enone chimera **4** is shown in (D) and a detailed view of the enone warhead bound to the β2 (TL) and β5 (ChTL) subunits are presented in (E) and (F), respectively. Ligands are contoured by the 2Fo-Fc omit maps at 1σ (blue net). A hemiketal adduct was trapped at the TL subunit binding compound **4** (E), unequivocally showing a 1,2 addition reaction of the Thr1Oγ to the enone carbonyl. In contrast, a cyclic adduct was found at the ChTL subunit (F). Differentiation between six (morpholine) and seven (oxazepine) membered ring adducts was possible by the use of enone **5** derivative, which contains an extra methyl group attached to the enone beta carbon. The superposition of morpholine (green) with oxazepine (light gray) modeled adducts is shown in (G) and a detailed view of **5** binding the ChTL subunit is shown in (H). The Fo-Fc difference map calculated from experimental data after modeling the oxazepine ring is contoured at 3σ (G). Positive and negative peaks are presented in green and red nets, respectively. Extra electron density near the wrong N-Cβ bond (red net) and missing density at the extra methyl position for morpholine ring possibility (green net) were found, indicating the correctness of the 6-membered morpholine ring as the final product. Sequence numbering is based on the primary sequence alignment of the respective yeast subunit with that of *Thermoplasma* (Löwe et al., 1995). Figures were generated with the Pymol software (Schroedinger). Oxygen, nitrogen, and sulfur atoms are shown in red, blue, and yellow, respectively.

step, followed by a second reaction leading to irreversible inhibition of the proteasome.

Enone **4** also exhibited this inhibition profile in the ChTL subunit, thus suggesting a similar stepwise reaction with the proteasome (Figures S1G–S1I). Compound **4** had a prolonged reversible phase, with reversible profiles at 2 and 6 hr of inhibitor incubation with the enzyme, indicating a less favored irreversible reaction step when compared to epoxyketones. We further measured the proteasome TL activity, showing that epoxyketones **1** and **3** are irreversible, whereas enone **4** is a reversible inhibitor of this proteasome catalytic unit (Figures S1J–S1L).

Taken together, these results suggest a different mode of proteasome binding for the α,β-unsaturated carbonyl system in compound **4**. Although one might anticipate the enone moiety of **4** to function as a one-step covalent irreversible inhibitor undergoing a 1,4-Michael reaction such as compound **2** (Groll et al., 2008), the reversible nature of the first step of inhibition observed for compound **4** precludes the possibility of a 1,4-addition, which would lead to an irreversible adduct. Furthermore, the binding data of enone **4** is similar to that observed for epoxyketone inhibitors **1** and **3**, showing a first reversible and a second irreversible reaction step with the proteasome ChTL subunit, thereby suggesting the likelihood of a 1,2-addition on the ketone of compound **4** as the first reversible step.

Crystal Structures

To characterize the binding modes of the carmaphycin derivatives, compounds **1**, **3**, and **4** were crystallized with the yeast 20S proteasome and diffraction data collected to 2.8 Å resolution (Figures 2 and S3). All three structures were refined to final Rfree values below 24.3% and root-mean-square deviation bond and angle values less than 0.006 Å and 1.0°, respectively (Table S1).

Using inhibitor concentrations in the millimolar range for crystal soaking, compounds **1**, **3**, and **4** targeted all three active sites of the proteasome through covalent linkages, establishing that they are catalytically active in the crystalline state (Figure S3A). The backbones of bound inhibitors were well defined as

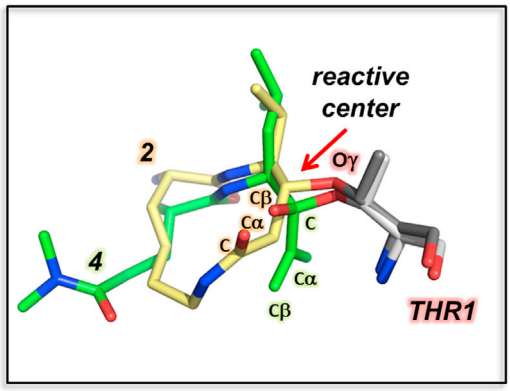

Figure 3. Detail of the Reactive Center of the Proteasome Catalytic Subunits as Found in the Crystallographic Structures of 2 and 4 in Complex with the 20S Proteasome

The Thr1Oγ is the general nucleophile, but the electrophile can vary depending upon warhead accommodation at the reactive center. The α,β-unsaturated amide and carbonyl systems of proteasome inhibitors **2** (pale yellow; Protein Data Bank ID 2ZCY) and **4** (green) are superposed at the TL (β2) catalytic unit. The Cβ of **2** is in prone position for an irreversible 1,4 addition type nucleophilic attack by Thr1Oγ. On the other hand, the carbonyl of **4** and the carbonyl of the natural peptide substrate (not shown) are positioned to undergo reversible 1,2 addition. Figures were generated with the Pymol software (Schroedinger). Oxygen, nitrogen, and sulfur atoms are shown in red, blue, and yellow, respectively.

antiparallel β sheets with contacts formed to the main chain atoms of residues Gly47N, Gly47O, Thr21N, Thr21O, and Ala49N as well as the side chain of Asp126 (Figure 2). The P1 leucine side chain was in proximity to the structurally rearranged Met45, as well as Ala20, Val31, and Ala49 in the S1 pocket. The methionine sulfoxide (via **1**) and *N,N*-dimethylglutamine (via **3** and **4**) P2 side chains were equally aligned and did not form any direct interaction with protein residues. The P3 valine residue was effectively stabilized in the S3 pocket by three alanine residues (Ala20, Ala22, and Ala27), whereas a hydrophobic cluster comprised of Pro104, Tyr106, Pro127, and Val128 accommodated the hexanoate tail in the ChTL (β5) and TL (β2) sites. This aliphatic group was exposed to solvent in the β1 subunit (caspase-like activity), where it adopts a random arrangement (Figure S3A).

Structural refinement and electron-density map calculations revealed that the epoxyketone inhibitors **1** and **3** bind to the Thr1 residue in a manner highly similar to that previously observed for epoxomicin (Groll et al., 2000; Huber et al., 2012) and its derivatives (Figure S3B). Unambiguously, a morpholine ring was formed between the catalytic Thr1 residue and the epoxyketone warheads (Figures 2A–2C), as a result of a two-step reaction between the protein and the inhibitors. As previously reported (Huber et al., 2012), the 1,2-addition of Thr1Oγ to the carbonyl carbon of the α′,β′-epoxyketone first occurs to form a hydrolysable hemiketal adduct. Subsequently, the epoxide group is prearranged for a nucleophilic attack by the Thr1 free N-terminal amine nitrogen. This reaction occurs at the C2 position of the epoxide and results in the final morpholine ring product (Figures 2A–2C), which is stabilized by interactions with Lys33Nε and Ser129Oγ.

Table 2. Interaction of the Proteasome Catalytic Center with the Natural Substrate and Inhibitors

Substrate/Inhibitor	Electrophile	Reaction	Nucleophile
Natural substrate	Carbonyl (C)	1,2-addition	Oγ from Thr1
Compound 1	Carbonyl (C)	1,2-addition	Oγ from Thr1
Compound 2	β carbon (Cβ)	1,4-addition	Oγ from Thr1
Compound 4	Carbonyl (C)	1,2-addition	Oγ from Thr1

Reaction types, nucleophiles, and electrophiles involved are described.

In contrast, enone **4** adopts two different ligand states in the crystal structure that give insight into the observed partial reversibility of **4** (Figures 2D–2F). The electron densities calculated for the TL subunit in the $2F_O$-F_C omit as well as in the F_O-F_C difference maps clearly displayed the attachment of **4** to Thr1Oγ via a hemiketal linkage involving the carbonyl group of the ligand (Figure 2E). The resulting alkoxide is stabilized in the oxyanion hole, interacting with the main chain of Gly47NH, similar to that observed in an epoxyketone-derived intermediate recently reported (Huber et al., 2012). The preference for a 1,2-addition over a 1,4-addition to the α,β-unsaturated system of **4** (Figure 2E) might be a consequence of warhead accommodation at the proteasome reactive center (Figure 3 and Table 2). Compound **4** positions the carbonyl of the enone in a position for nucleophilic attack by the Thr1Oγ nucleophile, thus enabling the 1,2-addition reaction. This scenario is different with **2**, which positions the β carbon of its α,β-unsaturated system at this reactive site, thus facilitating a 1,4-addition (Groll et al., 2008).

Structural inspection of the ChTL and caspase-like sites, on the other hand, revealed that enone **4** binds in an alternative mode at these catalytic centers (Figure 2F). Notably, **4** forms a cyclic adduct with the Thr1 residue involving both the ketone and alkene functional groups. Inspection of the diffraction data at 2.8 Å resolution and molecular fitting, however, did not unequivocally differentiate whether the cyclic product involved a 6-membered morpholine ring or a 7-membered oxazepine ring. Both adducts are structurally distinct and would involve different mechanistic paths. In a first hypothesis, the hemiketal intermediate of **4**, as observed in the TL subunit (Figure 2E), would undergo an unprecedented hydroamination reaction at the alkene residue with Thr1N. Depending on the regiochemistry of the reaction, two outcomes are plausible and would generate either morpholine or oxazepine adducts.

Formation of the oxazepine, however, could alternatively be achieved by a different reaction mechanism first involving a 1,4-addition of Thr1N to the enone followed by addition of the Thr1Oγ to the ketone (Figure S10). In this scenario the first covalent adduct would represent the irreversible product derived from 1,4-addition and the proteasome nucleophile would change from Thr1Oγ to Thr1N. Considering that Thr1Oγ is the general nucleophile reported in all proteasome covalent interactions to date, including the innate proteolytic mechanism (reviewed in Kisselev et al., 2012), and that Thr1N is protonated under physiological conditions, it is unlikely that Thr1N should act as the initial nucleophile. Furthermore, our reversibility experiments clearly show that **4** undergoes a stepwise reaction with the proteasome, in which the first step is reversible (Figures S1G–S1I). While this orthogonal mechanism is not consistent

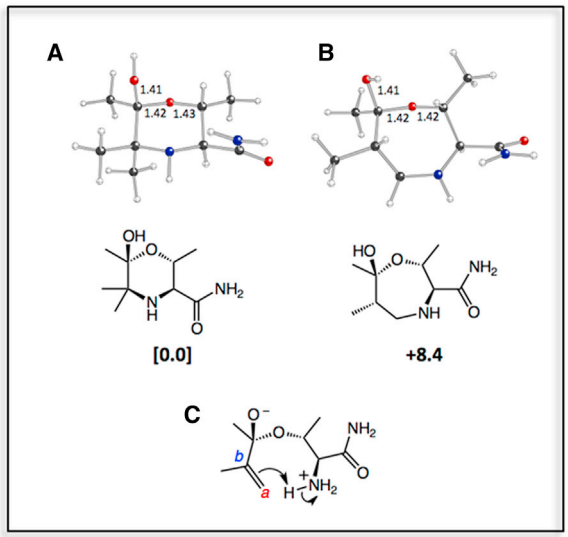

Figure 4. Quantum Chemical Calculations of the Regiochemistry of the ChTL Site Alkene Hydroamination of Inhibitors 4 and 5

(A and B) Computed structures (distances are approximate) of models for (A) the morpholine product and (B) a possible alternative oxazepine product and their computed relative free energies (kcal/mol).

(C) Model system used to examine proton transfer to carbon α versus carbon β. The transition state structure for proton transfer to Cβ is favored by 5 kcal/mol over that for transfer to Cα.

with our biochemical observations and with previously observed proteasome biochemistry, our structural data did not unequivocally rule it out.

To address this issue, we designed compound **5** as a structural probe to help discern between the six- and seven-membered ring formation scenarios. Compound **5** contains an additional carbon atom at the γ position of the enone. If the cyclized product was morpholine-based, then an ethyl side chain would be expected. On the other hand, an oxazepine-based adduct would be reflected by two adjacent methyl groups. The crystal structure of the proteasome bound to **5**, obtained at 2.5 Å resolution (Table S1), revealed a cyclized adduct occupying proteasome binding pockets similar to those observed with analogs **1**, **3**, and **4** (Figure 2H). Importantly, we clearly saw the telltale ethyl side chain in the $2F_O$-F_C omit map of **5** binding the proteasome (Figure 2H) and, further inspection of the F_O-F_C difference maps was consistent only with a morpholine cyclic product (Figure 2G). These data definitely exclude a 1,4-addition mechanism and reveal that the regiochemistry of the hydroamination reaction proceeds in a Markovnikov sense in generating the morpholine ring as final product.

Quantum Chemical Calculations

To further evaluate the reactivity of enone **4** with the proteasome, we modeled transition state structures for 1,2- and 1,4-addition as the first reaction step (Figures S4–S6), in the absence of the surrounding active site, using density functional theory calculations (M06-2X/6-31+G(d,p); see Experimental Procedures and Supplemental Experimental Procedures for details). The data indicate that the 1,2-addition (Figure S5) is favored over the 1,4-addition (Figure S6) by approximately 1 kcal/mol. We further investigated the regiochemistry of the ChTL site alkene hydroamination of **4** and **5**, by calculating the relative energies of both reaction products and transition state structures for formation of their carbocation precursors. These calculations indicate that **4** has an inherent thermodynamic and kinetic preference for morpholine over oxazepine ring formation (Figure 4). The morpholine product is predicted to be approximately 8 kcal/mol lower in free energy than the oxazepine product (Figures 4A and 4B). In addition, proton transfer (the first step in the hydroamination reaction) to the alkene CH_2 group is predicted to be favored over proton transfer to the more substituted carbon by 5 kcal/mol (Figure S9), as expected.

These theoretical calculations are in agreement with the experimental results, leading to a consistent mechanistic model in which the enone warhead in **4** undergoes an initial 1,2-addition, followed by hydroamination of the alkene, which occurs in a Markovnikov sense, leading to a morpholine ring as the final product.

DISCUSSION

As with the well-studied epoxyketone pharmacophore first described with the proteasome inhibitor epoxomicin (Groll et al., 2000), we show here that the enone functional group supports a two-step reaction leading to a cyclic adduct formation. The ketone groups of both electrophilic inhibitors are first attacked by the proteasome Thr1Oγ, followed by a second attack of the Thr1N on either the epoxy or alkene groups (Figure 5).

Based on the complementary results from our quantum chemical calculations and the crystallographic data obtained with compound **5**, we demonstrated that a morpholine ring, as observed in epoxyketone proteasome inhibitors, is also generated in the case of the enone pharmacophore. The general ligand binding in the proteasome-inhibitor complexes of epoxyketones **1** and **3** and enones **4** and **5** is identical (Figure S3), and markedly different to that observed in the **2**-derived proteasome complex (Groll et al., 2008; Figure 3). Consequently, the proteasome inhibition mechanism suggested for enones **4** and **5** is more similar to that verified for its parent scaffold-containing compounds **1** and **3** than to that for its parent warhead-containing compounds as in **2** and vinylsulfones (Kisselev et al., 2012; Figures 3 and 5).

Contemplating the reaction mechanism of the proteasome with inhibitor **4**, we considered several scenarios to dissect the mechanism of enzyme inhibition by this enone compound. First, the hemiketal intermediate is formed following the classical proteasome 1,2-addition mechanism involving the Thr1Oγ nucleophile and the inhibitor carbonyl, which is ideally positioned at the proteasome reactive center (Figure 3). After the formation of the hemiketal intermediate, the alkene residue is no longer activated. Thus, attack by the Thr1 amino group may proceed either directly with the isolated olefin (Figure 5C) or indirectly (Figure 5D).

While the aminolysis of epoxides is known to occur in water under mild conditions, the direct hydroamination of an inactivated alkene (Figure 5C), although thermodynamically feasible, generally requires a catalyst (Hultzsch, 2005). The geometric restrictions conferred by the hemiketal intermediate, however, should favor hydroamination, which is otherwise prohibited in

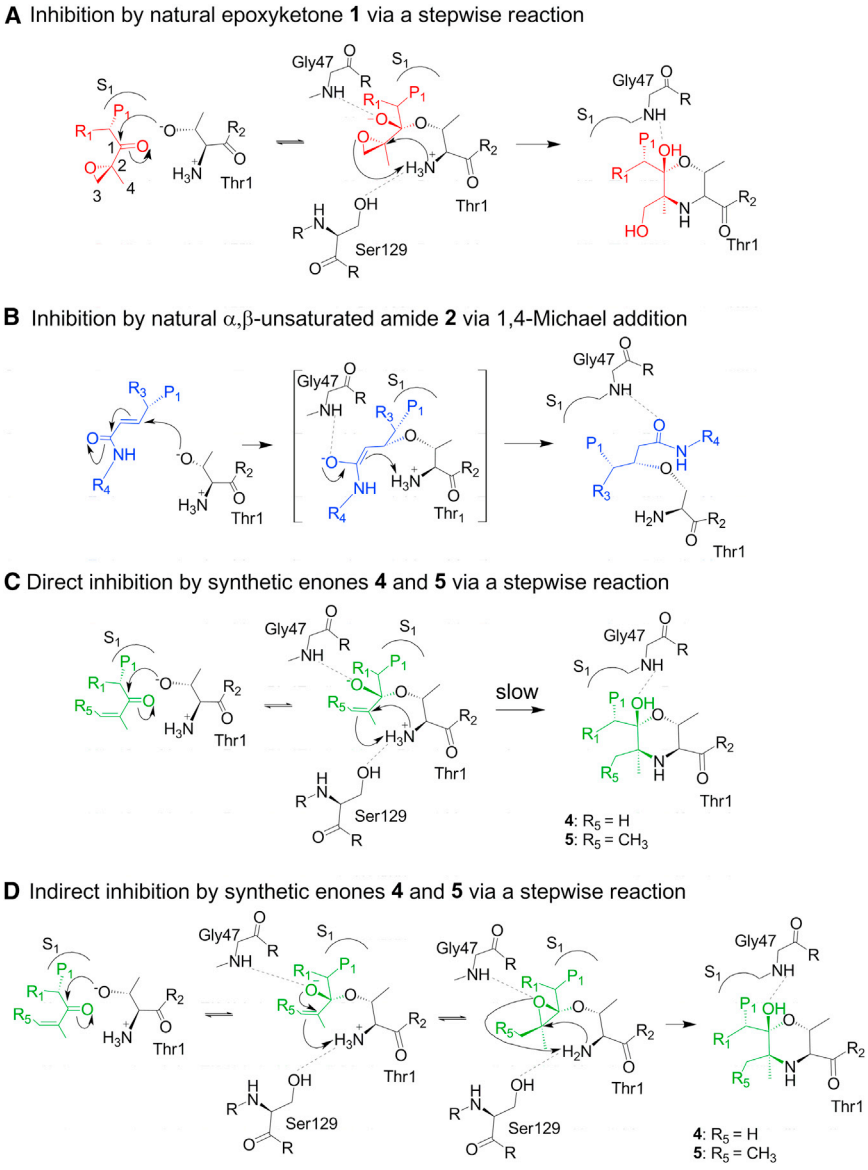

Figure 5. Proposed Reaction Mechanisms Involving the Proteasome Active Site Residue Thr1 and Inhibitors Containing Different Reactive Functional Groups

(A–D) Inhibitory reaction mechanisms are shown for (A) the epoxyketone warhead in epoxomicin (Huber et al., 2012, Wei et al., 2012) and **1**, (B) the natural α,β-unsaturated-amide system present in **2** (Groll et al., 2008), and (C and D) the enone warhead in the synthetic derivatives **4** and **5**.

solution. Direct hydroamination of the inactivated alkene may be facilitated by proton transfer from the free Thr1 amine to the C-C double bound, because the free amine is predicted to be protonated. The geometric restrictions conferred by the hemiketal bond and the overall ligand and warhead positioning in the enzyme binding pocket further reduce the entropic penalty for amine approach to the alkene π-bond. In addition, the Ser129Oγ side chain is approximately 3 Å from the Thr1 amine nitrogen atom in both cyclized and hemiketal adducts. Consequently, the placement of this residue at this proximate position may increase the nucleophilicity of the amine, thereby facilitating amine addition to the alkene (Schlummer and Hartwig, 2002).

An alternative mechanism involving an indirect hydroamination reaction is also plausible (Figure 5D). Here the hemiketal intermediate may first undergo an intramolecular rearrangement in which the generated alkoxide reacts with the adjacent olefin, the latter requiring activation by an acidic proton. This newly formed epoxide intermediate would then react with the free amine from Thr1 to complete the reaction and form the morpholine adduct. This mechanistic pathway is supported by quantum chemical calculations that predict barrierless formation of the epoxide intermediate (in the gas phase), and consequently, align the inhibitory mechanisms of the epoxyketone and enone functional groups.

Irrespective of the mechanistic route, the energetic barrier for the final step in the morpholine ring formation from the enone is expected to be greater than that of the epoxyketone, which may explain the decreased potency (Table 1) and partial reversibility of derivative **4** (Figure S1). Interestingly, when the functional group adjacent to the ketone is removed as in acylketone **6**, proteasome inhibition potency and cell activity are both abolished. This observation further suggests that the reactive epoxide and alkene functional groups are key to avoiding rapid hydrolysis of the initially formed hemiketal adduct. The nature of the warhead functional group and viability of the second reaction step to form an irreversible final product strongly contributes to the potency of these agents (Table 1). Although derivatives of **4** have not yet been observed in nature, recent biosynthetic studies of the epoxyketone proteasome inhibitors epoxomicin and eponemycin suggest the biosynthetic intermediacy of enone intermediates in those natural products that may foretell their future discovery (Schorn et al., 2014).

The modulated reactivity observed with compound **4** is somewhat reminiscent of the potent proteasome inhibitor fluorosalinosporamide, which also reacts with the proteasome in a two-step reaction mechanism involving a fast and reversible attachment to Thr1 followed by a slow and irreversible fluoride displacement reaction (Eustáquio and Moore, 2008; Groll et al., 2009). A major difference between these two inhibitors involves the nature of the reversibility of the initial proteasome adducts. In the case of fluorosalinosporamide, the β-lactone warhead is destroyed upon hydrolysis, whereas in compound **4**, the reverse reaction of the hemiketal intermediate would restore the reactive enone warhead.

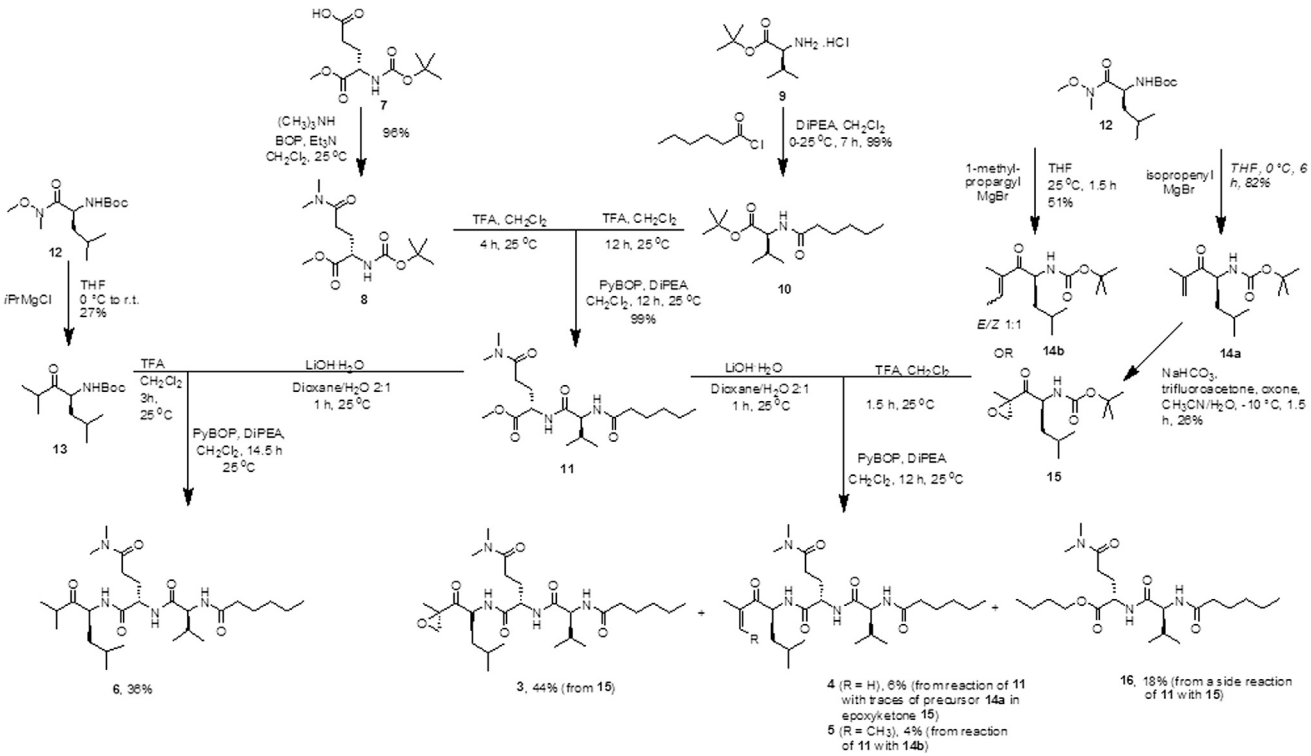

Figure 6. Synthetic Scheme Leading to Carmaphycin Analogs 3–6

The FDA approval of carfilzomib for treatment of multiple myeloma in 2012 sparks hope for a broader application of proteasome inhibitors as pharmaceutical agents, especially with regard to their unexploited potency for treatment of other cancer subtypes and immunological diseases. Although carfilzomib shows decreased side effects compared to bortezomib, it still suffers from its highly reactive warhead and toxic effects with prolonged use (Arastu-Kapur et al., 2011). Increasing the reversibility window with the newly established enone mechanism of action may be a promising approach to further improvements in this inhibitor class.

In summary, our data reveal that the α,β-unsaturated carbonyl systems in compounds **4** and **5** bind in an inverted orientation with respect to warhead positioning reported for **2**, thereby allowing for the initial attack on the carbonyl versus the conjugated alkene (Figures 3 and 5). This inversion of the innate chemical properties of the Michael-system can be ascribed to reactive group positioning for nucleophilic attack by Thr1Oγ (Figure 3). We demonstrated that the remaining alkene derived from the enone warhead of compounds **4** or **5** can undergo a second nucleophilic attack by proteasome Thr1N, leading to a cyclic morpholine adduct. Although this second reaction is slower, it is ultimately essential for inhibitor potency. We anticipate that alkene hydroamination could be exploited for enzyme inhibitor design in situations where a nucleophile and an acid are in proximity and under ideal geometric constrains to the target alkene, allowing for an otherwise entropically unfavorable reaction to yield a stable enzyme adduct.

SIGNIFICANCE

The proteasome is a validated biochemical target for cancer chemotherapy and is inhibited by natural products and synthetic molecules, following reversible or irreversible reaction mechanisms. The proteasome Thr1 catalytic residue actively participates in the inhibitory mechanisms through its side chain oxygen (Thr1Oγ) and its terminal amine (Thr1N) nucleophiles that attack the inhibitor's warhead electrophiles. We here report the crystal structures of the yeast 20S proteasome bound to carmaphycin and its derivatives containing epoxyketone and enone warheads, together with cell-based and mechanism-based assays. These data, along with quantum chemistry calculations, reveal previously unknown proteasome inhibitory biochemistry showing that the enone compounds are partially reversible and display promising biological properties. The proposed mechanism for the newly established enone proteasome inhibitor electrophile involves a two-step reaction, involving a 1,2-addition of Thr1Oγ to the ketone, followed by a hydroamination reaction of the inhibitor's inactivated alkene by Thr1N. This is an example of enzyme inhibition by hydroamination, and the suggested mechanism is well supported by the data presented. We were able to trap the reaction intermediate for the enone inhibitor in crystal structures, showing that warhead positioning in the enzyme active center is essential for defining the nature of chemical interactions with the Thr1Oγ nucleophile. In the carmaphycin derivatives series, the carbonyl moiety of epoxyketone

and enone warheads is ideally positioned for 1,2-addition of Thr1Oγ, resulting in a reversible hemiketal adduct as the first reaction product. The second reaction step involves the covalent attachment of Thr1N to the epoxide or to the alkene, following intramolecular aminolysis or hydroamination, respectively. Hydroamination is slower than aminolysis and represents a new chemical reaction for enzyme inhibition that allows for controlling the irreversibility of proteasome inhibitor binding.

EXPERIMENTAL PROCEDURES

Chemicals

All chemicals used in the present work were of reagent grade quality.

Crystal Structures

The 20S proteasome was purified from *Saccharomyces cerevisiae* as described previously (Gallastegui and Groll, 2012; Groll et al., 1997; Groll and Huber, 2005). Crystals were grown in hanging drops at 24°C, using a protein solution at 40 mg/ml in 10 mM morpholino-ethane-sulphonic acid (MES) pH 7.5 and EDTA (1 mM). Drops contained 1 μl of protein and 1 μl of the reservoir (30 mM of magnesium acetate, 100 mM of MES [pH 7.2] and 12% of MPD) solutions (Groll et al., 1997; Groll and Huber, 2005). Crystals were soaked with compounds **1**, **3**, **4**, **5**, or **6** at final concentrations ranging from 2 to 10 mM for 24 hr. Crystals were then transferred to a cryoprotecting buffer (30% 2-methyl-2,4-pentanediol, 20 mM magnesium acetate, 100 mM Tris [pH 6.9]) before cooling in liquid nitrogen.

Data collections were carried out at 100 K in a stream of liquid nitrogen gas (Oxford Cryo Systems). Crystals formed in the $P2_1$ space group with cell dimensions of about a = 135 Å, b = 301 Å, c = 144 Å and β = 113° (Table S1). Data to 2.5 Å were collected using synchrotron radiation with λ = 1.0 Å at the X06SA-beamline in SLS/Villingen/Switzerland. X-ray intensities and data reduction were evaluated using the XDS program package (Kabsch, 2010). Conventional crystallographic rigid body, positional, and temperature factor refinements were carried out with PHENIX (Adams et al., 2010) using the yeast 20S proteasome structure as starting model (Protein Date Bank accession code 3UN8; Huber et al., 2012). Cycles of maximum likelihood minimization, solvent modeling, and anisotropic correction were conducted in PHENIX (Adams et al., 2010), using grouped B-factor and noncrystallographic symmetry refinement. Real space refinement and inhibitor modeling were conducted using Coot (Emsley and Cowtan, 2004). Ligand construction, geometry file elaboration, and covalent ligand-protein linkage were carried out using JLigand (CCP4, 1994) and Avogadro software. The last step of refinement was performed in Refmac5 (Murshudov et al., 1997), using noncrystallographic symmetry and TLS refinement.

Omit maps were calculated using the program Omit (Bhat, 1988).

Inhibition Measurements

Inhibition assays of the purified 20S proteasome core particle from *S. cerevisiae* was conducted as previously reported (Pereira et al., 2012), with minor modifications. One nanomolar of proteasome was incubated with different inhibitor concentrations in Tris 25 mM pH 7.5; SDS 0.03%; EDTA 0.5 mM for 15 min at 37°C in 96-well plates, in a final reaction volume of 40 μL. Ten microliters of specific fluorogenic proteasome substrate Suc-LLVY-Amc (CTL substrate) or Ac-LRR-Amc (TL substrate) at 200 μM were added, resulting in a final substrate concentration of 40 μM. Samples were incubated for 15 min at 37°C and then the fluorescence in each well was measured. Fluorescence was normalized to the control conducted in the same conditions, however without inhibitor (related to 100% of enzyme activity), and plotted on a graph of inhibitor concentration versus remaining enzyme activity. The experimental data were fitted using the logistic four parameters equation in GraphPad software version 5 (GraphPad Prism).

Cell Assays

Cytotoxicity to H-460 human lung cancer and HCT-116 human colon cancer cell lines was determined as previously reported (Mevers et al., 2011; Gross et al., 2010; Tidgewell et al., 2010) with cell viability being determined by MTT reduction.

Reversibility Experiments

Yeast or human 20S proteasomes (10 nM) were incubated with 1 μM of inhibitor **4** or 0.01 μM of **1** or **3** for 2, 6, or 24 hr (yeast) or 1 hr (human) in Tris 100 mM pH 7.0. The proteolytic activity was measured with fluorescence, using ChTL (Suc-LLVY) or TL (Ac-LRR) 7-amino-4-methylcoumarin chromophoric substrates after 10-fold dilution of the protein and inhibitor. A control group maintained at the same experimental conditions but with constant initial inhibitor concentration ([**4**] = 1 μM or [**1**] or [**3**] = 0.01 μM) was performed for comparison. Protein activity in groups maintained at the same experimental condition, however in the absence of the inhibitor (DMSO control) was monitored to guarantee protein integrity during the different time points (Figures S1G–S1I in black). ChTL activity was stable up to 24 hr. However, TL catalytic activity was unstable in the incubation buffer after the first 4 hr; therefore, only data derived within the first 2 hr of incubation are reported for this latter enzyme activity.

Computational Details

All calculations were carried out using the M06-2X/6-31+G(d,p) method (Hohenstein et al., 2008; Zhao and Truhlar, 2008) with a continuum treatment for solvation (the SMD approach [Marenich et al., 2009], using chloroform, i.e., a solvent with a dielectric constant in the range of estimates for enzyme active sites), as implemented in Gaussian 09 (Gaussian). Explicit active site residues were not included in the calculations, so the preferences described here reflect inherent reactivity. Conformations of computed structures represent productive conformations for formation of the morpholine and oxazepine products. Structural drawings were produced using Ball & Stick (Müller et al., 2004). Computations on proton transfer did not include solvent and were carried out using the model system shown in Figure 4C in the main text. N–H and Ca/b–H distances were frozen to 1.30 Å for the two systems shown in Figure S9 and the remainder of each system was allowed to fully relax. The 5 kcal/mol energy difference discussed in the main text corresponds to the difference in electronic energies between these two optimized structures.

Synthesis

Compounds **7**, **9**, **12**, and **15** were synthesized as previously described (Pereira et al., 2012) and compounds **3–6** were synthesized according to Figure 6. Detailed synthetic procedures are reported in the Supplemental Experimental Procedures.

Optical rotations were measured on a JASCO P-2000 polarimeter. UV and infrared spectra were recorded on a Beckman DU800 spectrophotometer and on a Nicolet 100 FT-IR spectrometer, respectively. 1H, 13C, and two-dimensional nuclear magnetic resonance spectra were collected at a 1H resonance frequency of either 400 MHz (Varian Mercury), 500 MHz (Varian VX500), or 600 MHz (Bruker Avance III equipped with 1.7 mm and 5 mm TCI cryoprobes). Chemical shifts were calibrated internally to the residual signal of the solvent in which the sample was dissolved (CDCl3, δH 7.26, δC 77.0). High-resolution mass spectra were obtained on a ThermoFinnigan MAT900XL mass spectrometer or an Agilent Technologies 6530 Accurate-Mass Q-time-of-flight liquid chromatography/mass spectrometer. High-performance liquid chromatography was carried out using a dual Waters 515 pump system equipped with a Waters 996 photodiode array detector. Vacuum and flash chromatographic separations were performed using type H (10–40 μm, Aldrich) silica and silica gel 60 (40–63 μm, EMD), respectively. Merck thin-layer chromatography (TLC) sheets (silica gel 60 F254) were used for analytical TLC (aluminum-supported, layer thickness 200 μm) and preparative TLC (glass-supported, layer thickness 250 μm). All chemical reagents were obtained from Aldrich in an analytical or higher grade and were used as received unless stated otherwise. Solvents were acquired as high-performance liquid chromatography grade. All reactions were performed under dry nitrogen using glassware previously oven dried (150°C), unless otherwise specified. Glassware was allowed to reach room temperature under a flow of inert gas. Likewise, glass syringes and stainless steel needles, used to handle anhydrous reagents and solvents, were oven dried, cooled in a desiccator, and flushed with inert gas prior to use. Anhydrous THF was purchased from Aldrich or distilled from sodium/benzophenone; CH_2Cl_2 was distilled from CaH_2.

ACCESSION NUMBERS

The Protein Data Bank accession numbers for the proteasome binding compounds **1**, **3**, **4**, and **5** reported in this paper are 4HRD, 4HRC, 4HNP, and 4TLC.

SUPPLEMENTAL INFORMATION

Supplemental Information includes Supplemental Experimental Procedures, 30 figures, and 1 table and can be found with this article online at http://dx.doi.org/10.1016/j.chembiol.2014.04.010.

AUTHOR CONTRIBUTIONS

D.B.B.T. conducted the inhibition assays; D.B.B.T. and M.L.S. the mechanistic assays; D.B.B.T., M.L.S., and M.G. obtained the proteasome crystals, collected the diffraction data and solved the structures; W.H.G. and A.R.P. designed the compounds and with Y.K. synthesized the compounds; D.J.T. carried out the in silico experiments; T.B. and F.A.V. performed the cell experiments; B.S.M., W.H.G., A.R.P., and D.B.B.T. planned the experiments; all authors analyzed and discussed the results; B.S.M., D.B.B.T., and W.H.G. prepared the article with input from all authors.

ACKNOWLEDGMENTS

This research was generously supported by the NIH (CA127622 to B.S.M. and CA100851 to W.H.G. and F.A.V.), the German-Israeli Foundation for Scientific Research and Development (GIF 23 1102/2010 to M.G.), and the Sao Paulo Research Foundation (FAPESP 2011/21358-5 to D.B.B.T.).

Received: December 7, 2013
Revised: March 13, 2014
Accepted: April 22, 2014
Published: June 12, 2014

REFERENCES

Adams, P.D., Afonine, P.V., Bunkóczi, G., Chen, V.B., Davis, I.W., Echols, N., Headd, J.J., Hung, L.W., Kapral, G.J., Grosse-Kunstleve, R.W., et al. (2010). PHENIX: a comprehensive Python-based system for macromolecular structure solution. Acta Crystallogr. D Biol. Crystallogr. *66*, 213–221.

Arastu-Kapur, S., Anderl, J.L., Kraus, M., Parlati, F., Shenk, K.D., Lee, S.J., Muchamuel, T., Bennett, M.K., Driessen, C., Ball, A.J., and Kirk, C.J. (2011). Nonproteasomal targets of the proteasome inhibitors bortezomib and carfilzomib: a link to clinical adverse events. Clin. Cancer Res. *17*, 2734–2743.

Beller, M., Seayad, J., Tillack, A., and Jiao, H. (2004). Catalytic Markovnikov and anti-Markovnikov functionalization of alkenes and alkynes: recent developments and trends. Angew. Chem. Int. Ed. Engl. *43*, 3368–3398.

Bhat, T. (1988). Calculation of an OMIT map. J. Appl. Cryst. *21*, 279–281.

Borissenko, L., and Groll, M. (2007). 20S proteasome and its inhibitors: crystallographic knowledge for drug development. Chem. Rev. *107*, 687–717.

CCP4; Collaborative Computational Project, Number 4 (1994). The CCP4 suite: programs for protein crystallography. Acta Crystallogr. D Biol. Crystallogr. *50*, 760–763.

Emsley, P., and Cowtan, K. (2004). Coot: model-building tools for molecular graphics. Acta Crystallogr. D Biol. Crystallogr. *60*, 2126–2132.

Eustáquio, A.S., and Moore, B.S. (2008). Mutasynthesis of fluorosalinosporamide, a potent and reversible inhibitor of the proteasome. Angew. Chem. Int. Ed. Engl. *47*, 3936–3938.

Gallastegui, N., and Groll, M. (2012). Analysing properties of proteasome inhibitors using kinetic and X-ray crystallographic studies. Methods Mol. Biol. *832*, 373–390.

Goldberg, A.L. (2007). Functions of the proteasome: from protein degradation and immune surveillance to cancer therapy. Biochem. Soc. Trans. *35*, 12–17.

Groll, M., and Huber, R. (2005). Purification, crystallization, and X-ray analysis of the yeast 20S proteasome. Methods Enzymol. *398*, 329–336.

Groll, M., Ditzel, L., Löwe, J., Stock, D., Bochtler, M., Bartunik, H.D., and Huber, R. (1997). Structure of 20S proteasome from yeast at 2.4 Å resolution. Nature *386*, 463–471.

Groll, M., Kim, K.B., Kairies, N., Huber, R., and Crews, C.M. (2000). Crystal structure of epoxomicin:20S proteasome reveals a molecular basis for selectivity of α,β-epoxyketone proteasome inhibitors. J. Am. Chem. Soc. *122*, 1237–1238.

Groll, M., Schellenberg, B., Bachmann, A.S., Archer, C.R., Huber, R., Powell, T.K., Lindow, S., Kaiser, M., and Dudler, R. (2008). A plant pathogen virulence factor inhibits the eukaryotic proteasome by a novel mechanism. Nature *452*, 755–758.

Groll, M., McArthur, K.A., Macherla, V.R., Manam, R.R., and Potts, B.C. (2009). Snapshots of the fluorosalinosporamide/20S complex offer mechanistic insights for fine tuning proteasome inhibition. J. Med. Chem. *52*, 5420–5428.

Gross, H., McPhail, K.L., Goeger, D.E., Valeriote, F.A., and Gerwick, W.H. (2010). Two cytotoxic stereoisomers of malyngamide C, 8-epi-malyngamide C and 8-O-acetyl-8-epi-malyngamide C, from the marine cyanobacterium *Lyngbya majuscula*. Phytochemistry *71*, 1729–1735.

Hohenstein, E.G., Chill, S.T., and Sherrill, C.D. (2008). Assessment of the performance of the M05-2X and M06-2X exchange-correlation functionals for noncovalent interactions in biomolecules. J. Chem. Theory Comput. *4*, 1996–2000.

Huber, E.M., Basler, M., Schwab, R., Heinemeyer, W., Kirk, C.J., Groettrup, M., and Groll, M. (2012). Immuno- and constitutive proteasome crystal structures reveal differences in substrate and inhibitor specificity. Cell *148*, 727–738.

Hultzsch, K.C. (2005). Catalytic asymmetric hydroamination of non-activated olefins. Org. Biomol. Chem. *3*, 1819–1824.

Kabsch, W. (2010). Xds. Acta Crystallogr. D Biol. Crystallogr. *66*, 125–132.

Kisselev, A.F., van der Linden, W.A., and Overkleeft, H.S. (2012). Proteasome inhibitors: an expanding army attacking a unique target. Chem. Biol. *19*, 99–115.

Löwe, J., Stock, D., Jap, B., Zwickl, P., Baumeister, W., and Huber, R. (1995). Crystal structure of the 20S proteasome from the archaeon *T. acidophilum* at 3.4 Å resolution. Science *268*, 533–539.

Marenich, A.V., Cramer, C.J., and Truhlar, D.G. (2009). Performance of SM6, SM8, and SMD on the SAMPL1 test set for the prediction of small-molecule solvation free energies. J. Phys. Chem. B *113*, 4538–4543.

Meng, L., Mohan, R., Kwok, B.H., Elofsson, M., Sin, N., and Crews, C.M. (1999). Epoxomicin, a potent and selective proteasome inhibitor, exhibits in vivo antiinflammatory activity. Proc. Natl. Acad. Sci. USA *96*, 10403–10408.

Mevers, E., Liu, W.T., Engene, N., Mohimani, H., Byrum, T., Pevzner, P.A., Dorrestein, P.C., Spadafora, C., and Gerwick, W.H. (2011). Cytotoxic veraguamides, alkynyl bromide-containing cyclic depsipeptides from the marine cyanobacterium cf. *Oscillatoria margaritifera*. J. Nat. Prod. *74*, 928–936.

Molineaux, S.M. (2012). Molecular pathways: targeting proteasomal protein degradation in cancer. Clin. Cancer Res. *18*, 15–20.

Moore, B.S., Eustáquio, A.S., and McGlinchey, R.P. (2008). Advances in and applications of proteasome inhibitors. Curr. Opin. Chem. Biol. *12*, 434–440.

Müller, N., Falk, A., and Gsaller, G. (2004). Ball & Stick V.4.0a12, Molecular Graphics Application for MacOS Computers. (Linz: Johannes Kepler University).

Murata, S., Yashiroda, H., and Tanaka, K. (2009). Molecular mechanisms of proteasome assembly. Nat. Rev. Mol. Cell Biol. *10*, 104–115.

Murshudov, G.N., Vagin, A.A., and Dodson, E.J. (1997). Refinement of macromolecular structures by the maximum-likelihood method. Acta Crystallogr. D Biol. Crystallogr. *53*, 240–255.

Pereira, A.R., Kale, A.J., Fenley, A.T., Byrum, T., Debonsi, H.M., Gilson, M.K., Valeriote, F.A., Moore, B.S., and Gerwick, W.H. (2012). The carmaphycins: new proteasome inhibitors exhibiting an α,β-epoxyketone warhead from a marine cyanobacterium. ChemBioChem *13*, 810–817.

Schlummer, B., and Hartwig, J.F. (2002). Brønsted acid-catalyzed intramolecular hydroamination of protected alkenylamines. Synthesis of pyrrolidines and piperidines. Org. Lett. *4*, 1471–1474.

Schorn, M., Zettler, J., Noel, J.P., Dorrestein, P.C., Moore, B.S., and Kaysser, L. (2014). Genetic basis for the biosynthesis of the pharmaceutically important class of epoxyketone proteasome inhibitors. ACS Chem. Biol. *9*, 301–309.

Tidgewell, K., Engene, N., Byrum, T., Media, J., Doi, T., Valeriote, F.A., and Gerwick, W.H. (2010). Evolved diversification of a modular natural product pathway: apratoxins F and G, two cytotoxic cyclic depsipeptides from a Palmyra collection of *Lyngbya bouillonii*. ChemBioChem *11*, 1458–1466.

Wei, D., Lei, B., Tang, M., and Zhan, C.G. (2012). Fundamental reaction pathway and free energy profile for inhibition of proteasome by Epoxomicin. J. Am. Chem. Soc. *134*, 10436–10450.

Zhao, Y., and Truhlar, D.G. (2008). The M06 suite of density functionals for main group thermochemistry, kinetics, noncovalent interactions, excited states, and transition elements: Two new functionals and systematic testing of four M06 functionals and twelve other functionals. Theor. Chem. Acc. *120*, 215–241.